

Influence of Viscous Fingering on Dynamic Saturation–Pressure Curves in Porous Media

G. Løvoll · M. Jankov · K. J. Måløy · R. Toussaint ·
J. Schmittbuhl · G. Schäfer · Y. Méheust

Received: 15 February 2010 / Accepted: 12 July 2010
© The Author(s) 2010. This article is published with open access at Springerlink.com

Abstract We report on results from primary drainage experiments on quasi-two-dimensional porous models. The models are transparent, allowing the displacement process and structure to be monitored in space and time during primary drainage experiments carried out at various speeds. By combining detailed information on the displacement structure with global measurements of pressure, saturation and the capillary number Ca , we obtain a scaling relation relating pressure, saturation, system size and capillary number. This scaling relation allows pressure–saturation curves for a wide range of capillary numbers to be collapsed on the same master curve. We also show that in the case of primary drainage, the dynamic effect in the capillary pressure–saturation relationship observed on partially water saturated soil samples might be explained by the combined effect of capillary pressure along the invasion front of the gaseous phase, and pressure changes caused by viscous effects in the wetting fluid phase.

Keywords Drainage · Dynamic capillary pressure · Saturation · Water retention · Viscous effects · Rescaling

G. Løvoll (✉) · M. Jankov · K. J. Måløy
Department of Physics, University of Oslo, P.O. Box 1048, Blindern, 0316 Oslo, Norway
e-mail: grunde.lovoll@fys.uio.no

R. Toussaint · J. Schmittbuhl
Institut de Physique du Globe (IPGS), CNRS and University of Strasbourg (EOST),
Strasbourg, France

G. Schäfer
Laboratoire d'Hydrologie et de Géochimie de Strasbourg, UMR 7517 CNRS-Université de Strasbourg,
1 rue Blessig, 67083 Strasbourg Cedex, France

Y. Méheust
Geosciences Rennes (UMR CNRS 6118), Université Rennes 1, Rennes, France

G. Løvoll
Det Norske Veritas, Research and Innovation, Veritasveien 1, 1322 Høvik, Norway

1 Introduction

Different types of fluid displacements in porous media play important roles in many natural and commercial processes (Bear 1972; Dullien 1992; Sahimi 1995). Various multiphase problems have been studied and modelled over the last decades (see Bear 1972; Lenormand 1989; Dullien 1992; Sahimi 1995 and references therein).

The morphology of the displacement structures observed in immiscible two phase flow are in general controlled by the competition between viscous forces, gravitational forces and capillary forces; those various forces act on scales ranging from the pore scale to the system size. The relative wettabilities, viscosities and densities of the fluids, as well as the heterogeneity of the underlying porous media, could all play important roles in the competition process (Lenormand 1989; Måløy et al. 1985; Homsy 1987; Hulin et al. 1987; Birovljev et al. 1991; Måløy et al. 1992; Frette et al. 1997).

In order to characterize two phase flow in porous media, it is common practice to define a set of dimensionless numbers that quantify fluid pair characteristics. One such number is the viscosity ratio $M = \mu_{nw}/\mu_w$, where μ_{nw} is the dynamic viscosity of the non-wetting fluid and μ_w is the dynamic viscosity of the wetting fluid. The relative magnitudes of viscous and capillary forces (on the pore scale) are quantified by the *capillary number* Ca :

$$Ca = \frac{\mu_w v_f a^2}{\gamma \kappa} \quad (1)$$

where v_f is the Darcy velocity or specific discharge, a is the characteristic pore size, γ is the interface tension and κ is the intrinsic permeability of the homogeneous and isotropic porous medium. The specific discharge, or filtration velocity, v_f , is $v_f = Q/A$ where Q is the volumetric flow rate and A is the cross-section area perpendicular to the flow. In drainage, i.e. flow regimes where the non-wetting fluid replaces the wetting one, three limit flow regimes can be reached by tuning M and Ca (Lenormand et al. 1983, 1988; Lenormand 1989). If the flow rate is sufficiently low ($Ca \ll 1$), one reaches the capillary fingering regime (Lenormand et al. 1983; Lenormand and Zarccone 1985), for which the displacement structure is controlled solely by the fluctuations in the capillary threshold pressures. This regime is shown to have strong analogies to invasion percolation (Lenormand and Zarccone 1985; Chandler et al. 1982; Wilkinson and Willemsen 1983), and the invasion structure is fractal Mandelbrot (1982); Feder (1988) with a fractal dimension $D_c = 1.83 \pm 0.01$ (Lenormand and Zarccone 1985, 1989). If the invasion rate is high, the displacement is either stable or unstable depending on the viscosity contrast M . If a fluid with high viscosity is invading a fluid with low viscosity ($M \geq 1$), the resulting pressure field due to the viscous dominated displacement will act against the growth of the invasion front, leading to stabilization of the displacement front at a finite width (Saffman and Taylor 1958; Lenormand et al. 1988; Lenormand 1989; Frette et al. 1997; Xu et al. 1998). On the other hand, if the invading fluid is the less viscous one, the displacement is unstable and falls in the viscous fingering regime (Saffman and Taylor 1958; Måløy et al. 1985; Homsy 1987). The invasion structure is fractal with a fractal dimension $D_v \simeq 1.53$ (Måløy et al. 1985; Toussaint et al. 2005).

At intermediate capillary numbers, the viscous and capillary forces dominate on different length scales. At small scales capillary forces dominate the problem so that the invasion structure locally is that of capillary fingering, whereas viscous forces dominate the problem at larger scales, resulting in a morphology typical of viscous fingering at larger scales. The crossover length-scale between these two regimes l_c scales with the capillary number as:

$$l_c = \beta \frac{a}{Ca}. \quad (2)$$

Where the proportionality factor $\beta \simeq 1$ (Løvoll et al. 2004; Toussaint et al. 2005), in the following we will use: $l_c = a/\text{Ca}$. Note that this experimental result is different from the theoretical result for invasion percolation in a destabilizing gradient (Yortsos et al. 1997; Xu et al. 1998). Above this crossover length scale, the flow is destabilized by viscous forces and the displacement takes place in narrow-branched channels (for $M < 1$). Viscous fingering in disordered porous media is different from standard Saffman–Taylor fingering (Saffman and Taylor 1958), obtained in empty straight channels (Hele-Shaw cells), where the fingers are compact and occupy 1/2 of the system width W . In contrast, in disordered porous media these structures are branched, the invasion structure is fractal (Måløy et al. 1985) and it has been demonstrated that the invasion structure occupies a smaller fraction of the system ($0.4 W$) (Løvoll et al. 2004; Toussaint et al. 2005).

Many authors in the ‘physics community’ have been mostly concerned with characterizing and understanding displacement patterns and local flow properties. Hydrogeologists and soil scientists, on the other hand, have studied such systems with the goal of finding empirical laws relating saturation and capillary pressure at the Darcy scale, that is, a meso-scale at which the medium and the flow are described by continuous mathematical fields. The basic laws of multiphase flows treated at mesoscopic scale as a continuum require a closure of partial-flow Darcy relations. The key point of this closure is a functional relation between the capillary pressure (in a water–air system) and (water) saturation in the form of retention curves. The basic assumption underlying this continuous theory of multiphase flow is that for a given porous medium and a wetting-/nonwetting-liquid pair there is a well-defined relation between capillary pressure and saturation as found from quasi-static measurements on representative volumes. The best known mathematical models to describe the relationship are those of Leverett (1941), Brooks and Corey (1964) and Van Genuchten (1980). In these models, the model parameters are fit parameter and they are functions of the characteristics of the pore space, such as the pore size distribution and the degree of connectivity of the network. As found in the early 1960s, the retention curves may also depend on the direction and on the ‘displacement history’ of the water–air front, further on referred as hysteresis effects (Poulavissilis 1962; Mualem 1976, 1984; Kool and Parker 1987; Parker and Lenhard 1987; Luckner and Van Genuchten 1989; Lenhard et al. 1993; Stauffer and Kinzelbach 2001). Based on the parameterization procedure proposed by Parker et al. (1987), the known retention curves of a porous sample are often used to obtain capillary pressure–saturation curves for the different fluid pairs present in a multiphase system (e.g. Helmig 1997; Bohy et al. 2006). Later studies have demonstrated that hysteresis effects are not the only additional influence on this relationship and they show that there are considerable dynamic effects on the measured capillary pressure curves (Hassanizadeh and Gray 1988; Bourgeat and Panfilov 1998; Hassanizadeh et al. 2002; Dahle et al. 2005). Based on the results of former experimental studies Smiles et al. (1971), Stauffer (1977) and Hassanizadeh et al. (2002) suggested to account for dynamic effects on the retention curves by complementing the capillary pressure obtained under hydrostatic equilibrium conditions, depending on the water saturation of the soil sample, with a dynamic pressure term expressed by a lumped parameter times the variation of water saturation over time.

The present article addresses the gap between (i) capillary pressure as understood in the framework of a pore scale description and modeling of drainage, and (ii) capillary pressure as measured at the global scale of a sample or as described in Darcy-scale models. We present results from drainage experiments on synthetic quasi two-dimensional porous media, in which non-wetting air displaces a highly viscous wetting glycerol/water solution; hence, gravity has no influence on the displacement. We investigate the crossover regime between the regime of slow displacement (capillary fingering), and fast displacement (viscous

fingering). By using transparent quasi two-dimensional porous media as our porous media, optical methods are used to observe and analyse the local and global displacement geometry and how it changes with capillary number. The combination of local and global information allow us to perform *upscaling* of our data from the pore scale to the scale of our experimental porous media. In this manner, we are able to relate pressure, saturation, capillary number and system size.

2 Experimental Setup

The presented experiments are performed on quasi two-dimensional porous media. The thickness of the cells containing this porous medium is $a = 1$ mm, and corresponds to the diameter of the fixed glass beads composing the solid matrix of this porous medium. The porous medium is initially completely filled with a wetting liquid, which is displaced by a non-wetting fluid (primary drainage).

The porous medium is made of a random mono layer of glass beads: glass beads are poured on the sticky side of a contact paper (see Fig. 1). When the surface is completely filled with beads, excess beads are removed, leaving a random mono-layer of beads. The sticky paper is attached to a Plexiglas plate that has milled inlet and outlet channels 5 mm wide and 8 mm deep. The model is sealed off at the edges with silicon glue, thus forming a rectangular porous medium of width W and length L .

When glue is applied, another sticky paper is placed (glue down) on top of the glass bead layer. The resulting quasi two-dimensional porous medium can be filled with a liquid through the channels in the Plexiglas plate (see Fig. 1). The model is then placed (horizontally) with the beads down and clamped to a frame with an integrated pressure cushion. This pressure cushion ensures that the position of each bead is fixed and that the porous medium is always only one bead diameter thick (Fig. 1). The pressure cushion is filled with water and kept under hydrostatic pressure. The transparent model is placed and secured on top of a light-box. The porosity ϕ and intrinsic permeability κ are measured for all the models. Average values are: $\phi = 0.62 \pm 0.02$ and $\kappa = (0.017 \pm 0.002) \cdot 10^{-3} \text{ cm}^2$ ($\approx 1800 \pm 200$ Darcy).

The wetting liquid is either a 80–20% or a 90–10% by weight *glycerol–water* solution, dyed with 0.1% *Negrosine*, and the invading fluid is *air*. At room temperature, the wetting

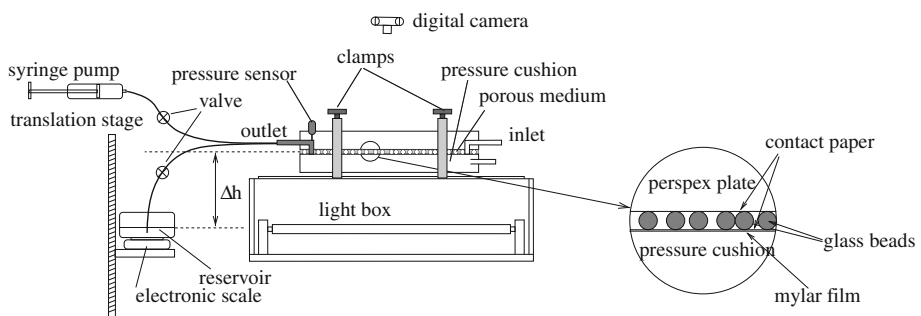


Fig. 1 Sketch of the experimental rig used for the flow experiments. The two-dimensional porous model is clamped to a light-box and kept in place by a pressure cushion

glycerol–water solutions have measured viscosities of $\mu_w \approx 0.050$ Pa.s and 0.165 Pa.s and densities of $\rho_w = 1,209$ and $1,235$ kg m⁻³, respectively. The corresponding parameters for the non-wetting air are $\mu_{nw} = 1.9 \cdot 10^{-5}$ Pa.s and $\rho_{nw} = 1.20$ kg m⁻³. The viscous ratio is thus $M = \mu_{nw}/\mu_w \sim 10^{-4}$, which is low enough to render the pressure gradient negligible in the non-wetting liquid. The surface tension (γ) between the two liquids is $\gamma_{BC} = 6.4 \cdot 10^{-2}$ N m⁻¹ (Vedvik et al. 1998). Two different liquid mixtures are used in order to tune the viscosity contrast of the fluids while maintaining the wetting properties. The 80–20% glycerol–water solution is used in the experiments presented in Sect. 3 while the 90–10% solution is used in the experiments presented in Sect. 4. In all experiments presented in Sect. 4, the temperature in the displaced wetting liquid is measured to enable control of the viscosity of the wetting liquid (and thus, of the capillary number).

The collected data consist of pressure measurements, pictures of the displacement structure and the extracted liquid volume. The absolute pressure in the wetting liquid is measured at the outlet channel (Fig. 1) using a *Honeywell 26PCA* or a *Sensor Technics 26PC0100 Flow Through* pressure sensor. Images are taken with a *Kodak DCS 420* or a *Nikon D200* digital camera. The extracted volume of wetting fluid is also recorded. All the data were collected and synchronized by a computer.

In this article, results from two model sizes are presented. All the experiments presented in Sect. 3, are performed on a model with $W = 200$ mm and $L = 350$ mm (called the *small model*). Besides this, in Sect. 4 we present results from a set of experiments for which $L = 840$ mm and $W = 215$ mm (called the *large model*).

Results from two fundamentally different types of experiments are presented: (i) quasi-static and (ii) constant flow rate experiments. In the first case, the flow is driven by slowly changing the pressure difference over the model. In the second case, a preset constant flow rate is imposed by means of a syringe pump or a tailored gravity pump (Méheust et al. 2002; Løvoll et al. 2004) (see Fig. 1). Since the observed structure is highly dependent on the imposed flow rate, the latter method has the advantage that invasion happens at a constant well-defined capillary number. This ensures that the length scales characteristic of the present flow regimes stay constant during the experiments (Løvoll et al. 2004; Toussaint et al. 2005).

3 Saturation–Pressure Relation: From Capillary Fingering to Viscous Fingering

As mentioned in the previous section, two different types of primary drainage experiments were performed. In the first set of experiments, the pressure difference across the model was controlled, and we performed slow (quasi-static) capillary fingering experiments. In the second set of experiments, a faster constant flow rate was imposed to investigate the transition to viscous fingering. This was done on the same model as the quasi-static experiments, using a syringe pump. This allowed to perform constant flow rate (Ca) experiments with the capillary number as tuning parameter. These two sets of experiments were carried out with the same porous model (of dimensions 1 mm × 200 mm × 350 mm), and will be presented in this section.

A third set of experiments, also at imposed capillary number, was performed, in which we analysed optically the invasion structure, simultaneously to the retention–saturation dependence. This was done in a larger model, of dimensions 1 mm × 840 mm × 215 mm. The results of these experiments and their treatment to obtain a model of the velocity dependence of the curves will be presented in Sect. 4.

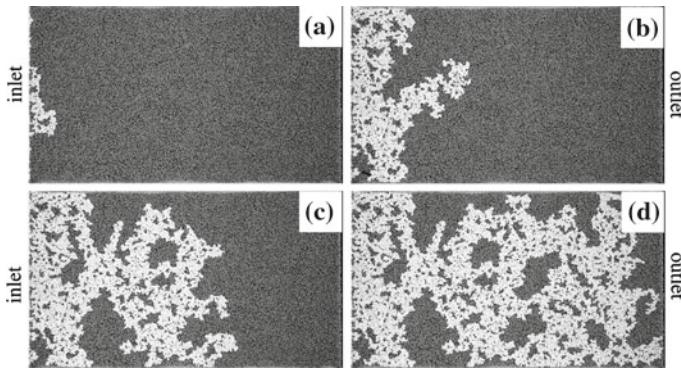


Fig. 2 Snapshots showing the evolution of a quasi static drainage experiment. The wetting glycerol–water solution is dark and the air appear as white. The experiment is driven by slowly increasing the pressure difference over the system. The snapshots **a**, **b**, **c** and **d** are taken at ~ 23.0 , 15.3 , 7.7 and 0 h before breakthrough, respectively. The total time from start to breakthrough was ~ 48 h. The snapshots are indicated in the saturation–pressure curve on Fig. 3

3.1 Quasi-Static Experiments Under Imposed Pressure Head

Figure 2 shows a selected set of images from a single quasi-static drainage experiment. The sequence a–d shows the invader from the start of invasion up to just before ‘break-through’, i.e. when the invader reaches the outlet channel. The invading cluster is typical of capillary fingering (Lenormand and Zarcone 1985), it spans the whole system width and leaves behind trapped droplets of wetting fluid, of various sizes (only limited by the system size). The snapshots in Fig. 2 are also referred to in the corresponding saturation–pressure curve in Fig. 3. In this experiment, the pressure drop over the system was changed slowly by keeping the atmospheric pressure at the inlet, while slowly lowering an open reservoir connected to the model outlet by tubes fully filled with the low compressible wetting fluid: this imposes a pressure drop corresponding to the hydrostatic pressure drop in the outlet tube (the vertically movable reservoir is indicated in Fig. 1). In order to minimize any additional pressure drop in the system due to fluid friction in the viscous fluid (dynamic effects), the reservoir is displaced vertically by small increments, and kept at rest between two successive increments until the fluids are not flowing anymore. At this point, the pressure at the setup outlet is constant and related to the atmospheric pressure P_{atm} and to the altitude of the reservoir (referenced with respect to the outlet’s altitude) through the law of hydrostatic pressure. As the setup inlet is open to the air, the pressure there is P_{atm} , so the deviation of the pressure at the outlet from the atmospheric pressure also happens to be the pressure head between the setup inlet and outlet. Since the viscosity of the air is negligible with respect to that of the liquid, that pressure head is also the sum of the capillary pressure and of the pressure head through the viscous liquid. This way of driving the system is what we call ‘quasi-static’. As described in the previous section, we measure the amount of liquid extracted from the model and the pressure at the setup outlet (gauge pressure sensor). From these mass measurements, the saturation of the non-wetting liquid (S_{nw}) is calculated as a function of time. By combining the calculated saturation with pressure measurements, a standard saturation–pressure curve is obtained. Pressure–saturation data from the experiment addressed in Fig. 2 are plotted in Fig. 3. As can be seen in Fig. 3, the pressure measurements exhibit notable fluctuations during the drainage process. The sudden

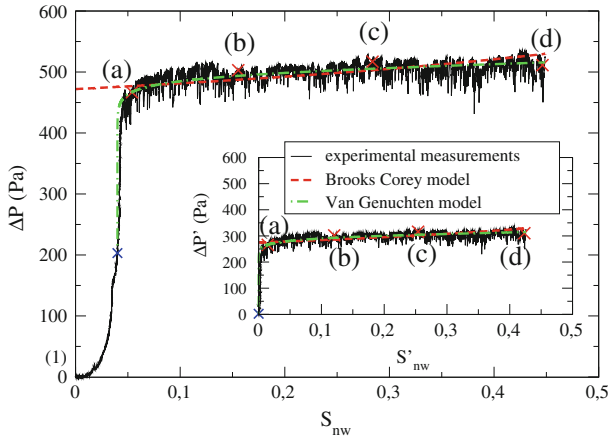


Fig. 3 Pressure–saturation curve from a quasi-static primary drainage experiment. The plotted pressure is the pressure difference over the model (from invasion front to outlet channel). The pressure was measured with a single gauge sensor in the outlet channel where the pressure recorded before the invasion process starts is used as reference. The plotted data were taken from the experiment shown in Fig. 2, the corresponding images are indicated by red crosses on the graph **a–d** from left to right. The subplot indicates the modified pressure and saturation, with a reference taken at the moment indicated by the blue cross, after the invader has filled a grain free buffer region in the Hele-Shaw cell, when the interface between the two fluids reaches the boundary of the granular medium. The two curves plotted are Brooks-Corey (*dashed*) and Van Genuchten (*dot-dashed*) models fitted on the data in the subplot—and reported on the main figure. This saturation–pressure curve seems consistent with a behaviour typical of soil samples

(random) jumps seen around the plateau corresponding to the hydrostatic pressures imposed by the reservoir happen during the dynamic stages, that is just after each displacement increment of the reservoir and before the flow has ceased, as the fluid interface (invasion front) penetrates new pores. During these dynamic stages, the measured pressure is different from that imposed at the setup outlet by the reservoir under static conditions. In order to invade a pore, the capillary pressure has to exceed the *capillary threshold pressure* for that pore throat. As this happens the capillary pressure decreases rapidly, the pore is filled with the invading fluid and the fluid interface in the surrounding pores retracts in order to adjust to the new capillary pressure. The size of these pressure jumps is random since the capillary thresholds are randomly distributed (Måløy et al. 1992; Furuberg et al. 1996). All pore necks in the system have an associated capillary threshold pressure. These threshold pressures are determined by the local pore geometry, the surface tension between the fluids, and the local wettability. Therefore, for a given porous medium and fluid pair the thresholds will have a given distribution. During drainage, a subset of this distribution is probed before the invader percolates the system (Auradou et al. 1999; Schmittbuhl et al. 2000; Auradou et al. 2003). If the experiment is driven by slowly increasing the pressure difference between the air and the liquid phase over the model, the invasion process starts once the pressure has reached the lowest pressure in the capillary threshold pressure distribution. For the data plotted in Fig. 3, this corresponds to the steep increase in pressure as air start invading the system. As the pressure is slowly increased further a larger portion of the threshold distribution becomes available for invasion, and while the pressure slowly changes, the non-wetting fluid invades the system and the saturation of non-wetting fluid increases, until the air percolates the system at breakthrough. Therefore, for ‘quasi-static’ experiments, relatively large changes in saturation occur for small pressure increases once the pressure is established at values well

inside the capillary threshold distribution. One can directly compare the pressure saturation curve of these quasi-static tests in grain-filled Hele-shaw cells to standard models from the hydrology literature: denoting the effective water saturation as

$$S_e = \frac{S_w - S_{wr}}{1 - S_{wr}} = \frac{1 - S_{nw} - S_{wr}}{1 - S_{wr}},$$

where S_{wr} is the residual water saturation, the Brooks–Corey model (Brooks and Corey 1964) is normally written as

$$p_c = p_d S_e^{1/\lambda},$$

where p_c is the capillary pressure of the soil sample at the Darcy scale and p_d is the air entry pressure. A least-square fit of the reduced data to this model is shown in Fig. 3. The corresponding fit parameters are: $p_d = 275$ Pa, $\lambda_{BC} = 3.1$, and $S_{wr} = 0$. Typically, for soils, λ stands between 0.2 and 3, the highest values corresponding to highly non-uniform grain-size distribution. The fact that we obtain a value close to the higher naturally occurring values, is consistent with the fact that the nearest neighbour distance, in such layers of beads put at random on a sticky plate, is certainly highly non-uniform compared to a three-dimensional packing of grains stacked under gravity. Given the value of the interfacial tension γ , the entrance pressure corresponds to a minimal curvature in the largest pore necks of $r_{\parallel} = \gamma/p_d = 0.25$ mm, which is of the order of a quarter of bead size: this is consistent with the expected order of magnitude for such a packing. The fact that S_{wr} is obtained at its smallest possible value, 0, can be explained by the fact that apart from the large fluctuations, no trend of any upward curvature of the pressure–saturation curve can be seen in Fig. 3.

Another common model for such curves is the Van Genuchten water retention function (Van Genuchten 1980),

$$p_c = \frac{1}{\alpha_{vg}} \left(S_e^{\frac{n}{1-n}} - 1 \right)^{\frac{1}{n}}$$

A fit to this model is shown as the dash-dotted curve in Fig. 3, and leads to Van Genuchten parameters $\alpha_{vg} = 0.0029$ Pa⁻¹ and $n = 9.9$. The value obtained for α_{vg} is consistent with that of a soil, the value of n is a few times larger than the one usually obtained for three-dimensional natural soils. This can be presumably attributed to differences in the packing, and notably the fact that the transition from the steeply growing part of the curve, up to point (a), into a plateau with fluctuations, is quicker than for many natural three-dimensional soils, most likely due to the fact that only one diameter of beads is represented in the packing. From a general point of view, it is interesting to note that this two dimensional medium presents a quasi-static pressure–saturation curve (and model parameters) somewhat similar to what could be expected for its three dimensional counterpart, and presumably represents well the processes at play in tests on opaque three-dimensional media.

3.2 Experiments Under Finite Imposed Flow Rate

As mentioned previously, we have also driven the system at constant capillary number by means of a syringe pump. In this case, a constant flow rate is imposed, and the pressure over the model will at any time be the pressure needed to maintain the flow rate. Figure 4 shows the saturation–pressure data curve for syringe pump driven experiments at different imposed flow rates. The black curve in Fig. 4 shows a slowly driven experiment, at $Ca = 0.01$. It exhibits the same initial pressure buildup in the beginning of the experiment as for the ‘quasi-static’ experiment (Fig. 3). When the average capillary threshold pressure is reached

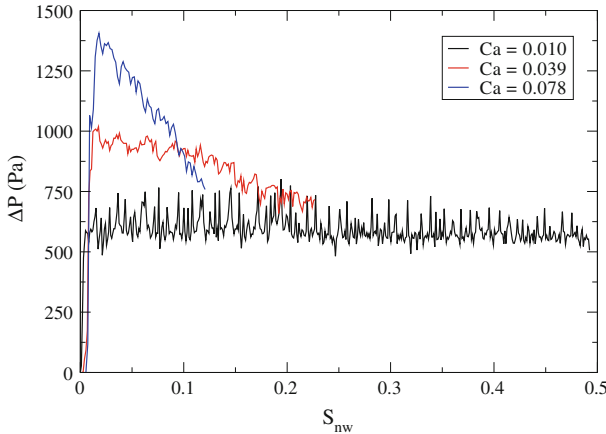


Fig. 4 Saturation–pressure curves from three primary drainage experiments on the *small* model, driven at constant flow rate (constant Ca) by a syringe pump. S_{nw} is the saturation of the system in the non-wetting fluid (air), related to the saturation in wetting fluid (water–glycerol) S_w by $S_{nw} = 1 - S_w$. The total duration of the drainage experiments are ~ 2.4 h, ~ 10 min. and ~ 3 min for $Ca = 0.010, 0.039$ and 0.078 , respectively

the pressure fluctuates more strongly around this constant value during the whole drainage process. The two other curves shown in Fig. 4 present similar results for faster syringe pump driven experiments. These curves still show the random pressure fluctuations caused by the variation of capillary pressure thresholds. Additionally, compared to quasi-static drainage curves, the slope of the drainage curve is ‘reversed’ by the boundary conditions imposed on fluid velocities (constant flow rate): after the initial pressure buildup, the pressure is steadily decreasing while the air saturation increases. This feature was also observed with different boundary conditions in some numerical studies of dynamic fingering (Dahle et al. 2005). As already known and shown in other studies (Hassanizadeh et al. 2002; Dahle et al. 2005), we observe here that for a given porous medium there is no one-to-one relation between the saturation and the pressure over the system. Boundary conditions and dynamic effects have a significant impact on the pressure versus saturation relation. In the next section, we shall look at dynamic effects more closely.

4 Relating Capillary Number, Saturation, Pressure and System Size

We now turn to the results from experiments carried at different imposed flow rate on the large model (1 mm × 215 mm × 840 mm). Dynamic capillary pressure as measured in water retention experiments (Hassanizadeh et al. 2002) is often defined as the total pressure difference over the porous medium (ΔP), or some spatial average of the pressure over one of the present phases (Dahle et al. 2005) (see discussion in Sect. 5). The total pressure difference is a combination of capillary pressure along the invasion front (P_c) and the pressure head caused by viscous effects (ΔP_v) (Washburn 1921)

$$\Delta P = P_c + \Delta P_v \tag{3}$$

In drainage, the capillary pressure is essentially unaffected by the speed of the flow and system size (Méheust et al. 2002), except in details, since the pores invaded are not exactly the same (this is, however, not the case in fast imbibition, see (Weitz et al. 1987)). The order

of magnitude of this capillary pressure does not change in time and as demonstrated in Sect. 3 it can be treated as randomly fluctuating around a well-defined average value. However, the viscous part (ΔP_v) is dependent on finite size effects and invasion speed. In the following, the reported measured pressure (P) is, therefore, equal to the viscous pressure drop:

$$P = \Delta P_v \quad (4)$$

It is obtained from our measurements by using the pressure just before breakthrough (t_{bt}) as reference null pressure $P(t_{bt}) \equiv 0$.

In Fig. 5, snapshots of the invasion structure are shown for four different drainage experiments. The experiments are all performed at constant flow rate and the snapshots are such that the viscous pressure drop (P) across the cell is the same in all snapshots. These pictures do also illustrate how the saturation of the non-wetting liquid changes with capillary number.

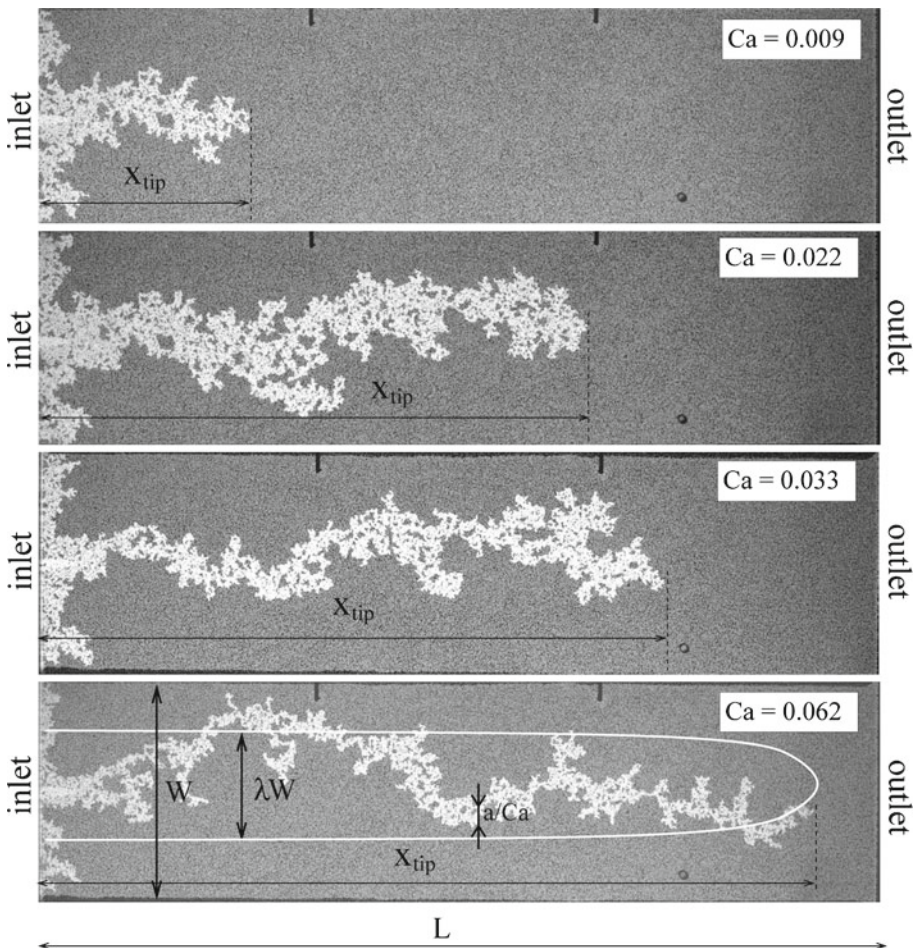


Fig. 5 Images of experiments taken at different withdrawal rates (expressed by the capillary numbers). The viscous pressure difference over the model is $P \sim 490$ Pa in all the pictures. The invasion structure is initiated in the center of the flow cell by creating a small ‘notch’ in the porous medium at the centre of the inlet. On the lower image relevant length scales are indicated

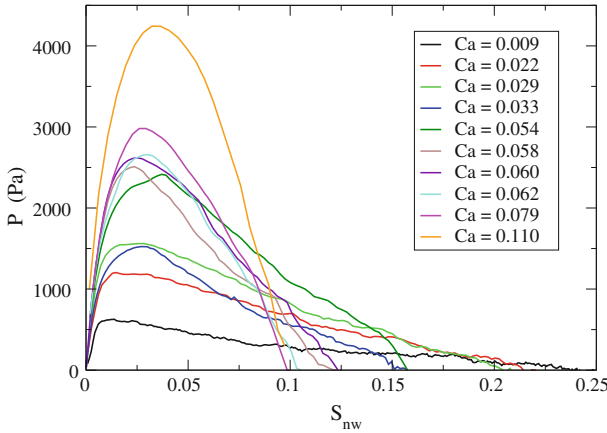


Fig. 6 Pressure (see Eq. 4) as a function of the non-wetting fluid saturation (S_{nw}) for some experiments on the *large* model. The initial pressure buildup is due to inertia in the liquid. The effect is explained in Appendix A

As the invasion rate increases, the invasion structure gets thinner, which again leads to lower saturation of the invading non-wetting liquid. The pressure versus air-saturation (S_{nw}) plots for these drainage experiments are shown in Fig. 6. After the initial pressure buildup, these experiments show the same behaviour as the two ‘fast’ syringe driven experiments in the previous section (Fig. 4).

If the system is big enough, viscous effects will always dominate the problem at larger length scales. The crossover length scale is given by Eq. (2), $l_c = a/Ca$. Above this length scale, the viscous pressure drop dominates over capillary threshold fluctuations and the displacement dynamics is in the viscous fingering regime. Where displacement will take place in narrow channels and branched loop-less structures, as shown in Fig. 5 (Løvoll et al. 2004; Toussaint et al. 2005). At scales below this, capillary fluctuations dominate the dynamics, and the resulting structure is characteristic of the capillary fingering regime, with droplets of wetting fluid remaining trapped in loops of the invading non wetting fluid. Looking at pictures from four experiments at different speeds and at the same P (Fig. 5), it is obvious that the viscous pressure drop is related to the position of the most advanced finger and the capillary number. Earlier studies have also shown that the invasion structure is screened by the advancing invasion front and that the propagation speed of the invasion front is fairly constant (Løvoll et al. 2004; Toussaint et al. 2005). The process is thus stationary in a referential attached to the advancing finger tip. All the invasion happens in a zone close to this tip. As was obtained in a detailed analysis of the pressure field, measuring at several points around the invader in each experiment (Løvoll et al. 2004), the pressure is roughly constant behind the finger tip, and the viscous pressure gradient in front of the invasion structure is essentially constant. The viscous pressure is thus (to the first order) a linear function of the distance from the outlet to the most advanced finger:

$$P = \overline{\nabla P}(L - x_{tip}) \tag{5}$$

where $\overline{\nabla P}$ is the average viscous pressure gradient and x_{tip} is the tip position of the most advanced fingertip (indicated on Fig. 5). $\overline{\nabla P}$ can be approximated by Darcy’s law:

$$\overline{\nabla P} = \frac{\mu_w v_f}{\kappa} \tag{6}$$

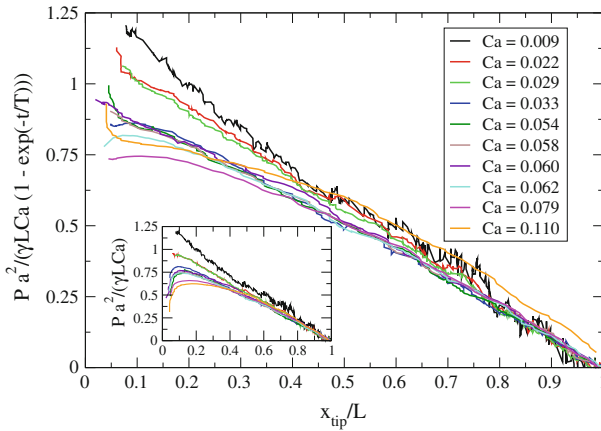


Fig. 7 Data collapse of pressure data as function of x_{tip}/L , where the initial pressure buildup is corrected with the method outlined in Appendix A using $T = 114$ s. The inset shows scaled pressure data without initial pressure correction

Consequently, we can write the pressure change caused by viscosity effects as:

$$P = \frac{\mu v_f}{\kappa} (L - x_{tip}) = \frac{\gamma Ca}{a^2} (L - x_{tip}), \tag{7}$$

where we have used the expression of the capillary number, Eq. 1. This allows to express the ratio of x_{tip} to the system length L as a function of pressure and capillary number:

$$1 - \frac{x_{tip}}{L} = \frac{a^2}{\gamma L Ca} P \tag{8}$$

where we recall that P is the measured viscous pressure drop over the system (see Eq. 4).

In the inset of Fig. 7, the rescaled pressure $a^2 P / (\gamma L Ca)$ is plotted as a function of the reduced finger tip position x_{tip}/L for a range of capillary numbers. The pressure drop across the model can also be corrected for the inertia of the fluid during the initial acceleration. In Appendix A, we show how these initial inertial effects lead to a multiplicative factor $(1 - e^{-t/T})$ for the time-dependent pressure, where T is the time characteristic of the initial pressure buildup. A way to correct for these inertial effects is then, after the determination of T by a least square fit, to represent the corrected pressure $P/(1 - e^{-t/T})$ rather than the measured pressure. This is shown in Fig. 7. Based on the argument above, we introduce the dimensionless reduced pressure:

$$P^* \equiv P \frac{a^2}{\gamma L Ca} \left(1 - e^{-t/T}\right)^{-1} = 1 - \frac{x_{tip}}{L} \tag{9}$$

Using our knowledge of the morphology of the invading cluster in the transition from viscous- to capillary-fingering (Løvoll et al. 2004; Toussaint et al. 2005), a relation for the non-wetting liquid saturation (S_{nw}) as a function of finger tip position x_{tip} , capillary number (Ca) and the width of the system W can also be derived. This is done by counting the number of invaded pores N_{inv} as a function of x_{tip}/L . Earlier studies (Løvoll et al. 2004; Toussaint et al. 2005) have shown that the invasion typically takes place in a limited region in the center of the channel. The width of this region is λW , where W is the width of the system and $\lambda \simeq 0.4$. Above this scale, we have a linear channel where the displacement structure

could be considered homogeneous. Inside this channel (of width λW), two flow regimes are present depending on the length scale considered. At large scales (between λW and l_c) the flow structure is that of viscous fingering, which is a treelike structure with branches and no loops. The viscous fingering structure is a fractal with a fractal dimension $D_v \simeq 1.53$ (Toussaint et al. 2005). At smaller scales, capillary forces dominate the flow process and the displacement structure is that of capillary fingering. Capillary fingering is also fractal, with fractal dimension $D_c \simeq 1.83$ (Wilkinson and Willemsen 1983; Lenormand and Zarcone 1985). The relevant length scales in the problem are sketched in Fig. 5. The argument below is thus valid when:

$$a \ll \frac{a}{Ca} = l_c \ll \lambda W \tag{10}$$

When the most advanced finger tip is at x_{tip} , the invasion has taken place in a channel of area $\lambda W x_{tip}$. This channel is composed of $x_{tip}/(\lambda W)$ square zones of linear size λW . In each of these zones the invading viscous fingering structure goes through $(\lambda W Ca/a)^{D_v}$ square boxes of linear size a/Ca . And in each such box, the invader occupies on average $[(a/Ca)/(\alpha a)]^{D_c} = (\alpha Ca)^{-D_c}$ pores of linear size αa , with α a geometrical pre factor, of order of magnitude 1 (indicating that the average pore volume is *not* exactly a^3 but rather $(\alpha a)^3$). The total number of invaded pores is thus:

$$\begin{aligned} N_{inv}(x_{tip}) &= \frac{x_{tip}}{\lambda W} \left(\frac{\lambda W Ca}{a} \right)^{D_v} (\alpha Ca)^{-D_c} \\ &= \frac{x_{tip} (\lambda W)^{D_v-1}}{a^{D_v}} \alpha^{-D_c} Ca^{D_v-D_c} \end{aligned} \tag{11}$$

The total volume accessible to the fluid is $WLa\phi$ and the average pore volume is $(\alpha a)^3$. The saturation of the non-wetting fluid, S_{nw} , can thus be written as:

$$\begin{aligned} S_{nw} &= \frac{N_{inv}(\alpha a)^3}{WLa\phi} \\ &= \frac{x_{tip}}{L} \frac{a^{2-D_v}}{\phi} \frac{(\lambda W)^{D_v-1}}{W} \alpha^{(3-D_c)} Ca^{D_v-D_c} \end{aligned} \tag{12}$$

This relation can be inverted to obtain a dimensionless reduced saturation S^* which is a reduced variable of the tip position, x_{tip}/L . It relates to the dimensional saturation of the wetting fluid, S_{nw} , according to:

$$S^* \equiv \frac{x_{tip}}{L} = S_{nw} \alpha^{(D_c-3)} \frac{\phi}{\lambda^{D_v-1}} \left(\frac{W}{a} \right)^{2-D_v} Ca^{D_c-D_v} \tag{13}$$

Based on Eqs. 9 and 13, we predict that P^* and S^* are related through the relation:

$$P^* = 1 - S^* \tag{14}$$

This is indeed the case to a large extent, as shown in Fig. 8. The satisfactory character of this data collapse for the reduced pressure drop versus reduced saturation at various speeds can be seen when comparing Fig. 8 to the raw data presented in Fig. 6. In addition, the above arguments can be applied to the particular state $P^* = 0$, i.e. at breakthrough, when the invading non wetting fluid reaches the outlet, at $x_{tip} = L$. The saturation reached at this time gives the final saturation which can be retrieved before the invader reaches the outlet, and thus gives an estimate of the efficiency of the invasion process before breakthrough.

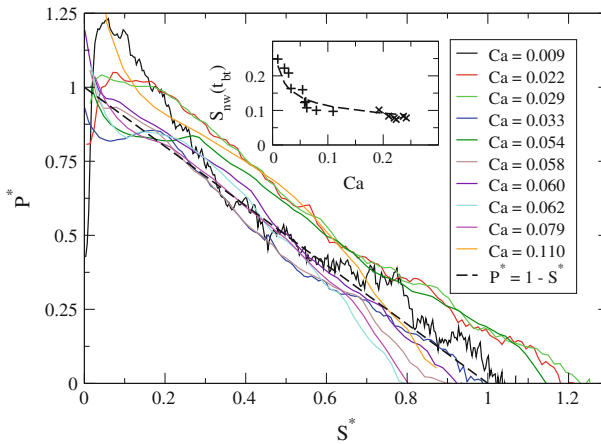


Fig. 8 Data collapse of saturation versus pressure curves from experiments performed at capillary numbers between $9 \cdot 10^{-3}$ and $1.1 \cdot 10^{-1}$. The collapse is obtained by plotting P^* as a function of S^* . The collapse is consistent with the prediction in Eq. 14; it is indicated by the *dashed line*. Compare this to the original data shown in Fig. 6. The only ‘free parameter’ in the data collapse is the geometrical pre-factor α , $\alpha = 0.75$ is used in the collapse. The *inset* shows the saturation of the non-wetting fluid (S_{nw}) at breakthrough time (t_{bt}) as a function of the capillary number. The *dashed line* in the inset is the breakthrough saturation predicted by Eq. 15

This point corresponds to the prediction $S^* = 1$, i.e. according to Eq. 13, to a final non-wetting saturation S_{nw} at breakthrough

$$S_{nw}(t_{bt}) = \alpha^{(3-D_c)} \frac{\lambda^{D_v-1}}{\phi} \left(\frac{a}{W}\right)^{2-D_v} Ca^{D_v-D_c}. \quad (15)$$

and a water residual saturation $S_w = 1 - S_{nw}$ that reads accordingly. This prediction for the final air saturation as a function of the speed of the invasion process Ca is shown in the inset of Fig. 8 as a dashed curve. The measurements of the final invader saturation at breakthrough for experiments carried out at various capillary numbers, represented as the crosses, are in good agreement with this prediction.

5 Discussion

The theory leading to the scaling relation between pressure and saturation in Eq. (14) is valid for a limited range of capillary numbers, for high viscous contrast and for systems without gravity. The limits in capillary numbers are given in Eq. 10. We believe that the upper limit in capillary number is $Ca \approx 1/10$ which implies that our largest reported capillary number $Ca = 0.11$ is close to this limit. For higher capillary numbers, the width of the viscous fingers is close to the pore scale and there is no capillary fingering structure at smaller scales. This would imply that the saturation is independent of the capillary number at higher flow rates and is constant for all Ca higher than the ones satisfying Eq. (10). This observation is consistent with the measured breakthrough saturation shown in the inset of Fig. 8 where the saturation level seems to be fairly constant for capillary numbers above ~ 0.1 . At the other end of the scale range, it is the size of the system that sets the limit. When the capillary number is low enough for the crossover length scale to reach the system width ($l_c \approx \lambda W$) (see Fig. 2),

there is no crossover from capillary to viscous fingering: a constant breakthrough saturation is obtained. In our case, this corresponds to $Ca \approx 1/100$ which is of the order of the smallest presented capillary number.

It should also be noted that the invading cluster is fractal for all capillary numbers and the saturation, therefore, depends on the width W . At finite flow rates, the system size determines the importance of viscous effects (dynamic effects). A given capillary number Ca will result in a crossover length scale $l_c = a/Ca$. Above this length scale viscous effects will dominate the problem. This observation raises a question on the general validity of the *representative elementary volume (REV)* assumption commonly used in Darcy scale modeling.

The data collapse of experimental measurements presented in Fig. 8 displays a certain dispersion. The quality of this collapse becomes evident when it is compared to the raw saturation–pressure data shown in Fig. 6. Figure 7 shows that the collapse of the pressure data is good, so the main scatter in the collapse of Fig. 8 results from the saturation data. Even if there is scatter in the saturation data, we will claim that no systematic trend is visible. The experiments are carried out on disordered media, and the morphology of the invasion structures are statistically fractals. On such a small systems, noise is expected. For these model systems there are also boundary effects at the inlet and outlet. The arguments leading to Eq. 12 assume that the process is stationary, and they do not take boundary effects into account. If one looks at Fig. 5, it is evident that there are boundary effects near the inlet channel and that the saturation there is different from the saturation further into the model. In addition to this, the saturation in the frontal region is different from the stationary part left behind the advancing front, so when the invasion front reaches the outlet channel, the saturation will be lower in the vicinity of that channel than the saturation away from it. Earlier studies (Løvoll et al. 2004; Toussaint et al. 2005) have shown that the size of the active frontal region is of the order of the system width. At breakthrough there is, therefore, a region at a distance $\propto W$ where the saturation is lower than in the ‘completely invaded’ parts of the system. It is, therefore, crucial that the system be large enough to average out these fluctuations and minimize end effect. Therefore, when designing such experiment, we would suggest that one ensures that $L \geq 4W$ and in addition that the system be wide enough so that the Eq. 10 allows for a sufficiently large range of available capillary numbers.

As said earlier, the pressure (or dynamic capillary pressure) is often measured between two points, one in one phase, the other in the other one. Commonly, this is done practically at the inlet and outlet. However, some authors (Hassanizadeh et al. 2002; Dahle et al. 2005) define the dynamic capillary pressure as being the difference between the (spatial) average pressure in one phase, and the average pressure in the other one. Although this definition is easy to use in a numerical system, it is difficult to use in practice in an experimental system, where the pressure in the two phases is normally known only at a limited set of measurement points. We have measured (Løvoll et al. 2004; Toussaint et al. 2005) that the pressure in the wetting liquid is roughly spatially linearly decreasing in front of the invading tip, and roughly constant (equal to P_c) on the sides behind the tip, this is an approximation, see (Løvoll et al. 2004) for details of the pressure modeled and measured around the air fingers. The pressure in the continuous air phase is roughly constant. Consequently, the spatial average of the air pressure is P_{atm} , and the average pressure in the wetting phase is dominated by the pressure ahead of the tip, i.e. the term

$$\int_{x_{tip}}^L dx \left(P_{atm} + P_c + P \cdot \frac{x - x_{tip}}{L - x_{tip}} \right) / \left(\int_{x_{tip}}^L dx \right) = P_{atm} + P_c + P/2.$$

Here, this difference between the average pressures in both phases average should be around

$$P/2 + P_c,$$

when the measured total variation across the cell is

$$\Delta P = P + P_c.$$

Both should be qualitatively the same in terms of dependence on the flow speed, system size, etc. As with the measurements presented here, the ‘dynamic capillary pressure’ is expected to be system size dependent. In our case, the invading structure is screened from the viscous pressure field by the active zone near the most advanced finger (Løvoll et al. 2004). This implies that in the frontal region there is a spatial trend in the capillary pressure along the fingers: the capillary pressure in the fingertips (where invasion is happening) is larger than further back. This has been reported in earlier studies (Løvoll et al. 2004), and the effect is also present in the classic Saffman–Taylor solution (Saffman and Taylor 1958).

It is also interesting to note that the models proposed by the authors of references Hassanizadeh et al. (2002) and Dahle et al. (2005) include a linear dependency of the time derivative of the saturation ($\partial S/\partial t$) in the definition of the ‘dynamic capillary pressure’. It is important to mention that for a system of volume V and porosity ϕ , $\partial S/\partial t = Q\phi/V$, so that $\partial S/\partial t \propto Ca$. This effect, reported by Hassanizadeh et al. (2002) and Dahle et al. (2005), is indeed a viscous effect (Niessner and Hassanizadeh 2008), and for high viscous contrasts the proportionality factor has been derived in Sect. 4.

In the scaling theory developed in Sect. 4, the invader morphology at small scales is used to predict ‘Darcy scale’ behaviour. We, therefore, believe that this type of argument could be very useful for Darcy scale modeling. Our results also demonstrate that for flow conditions where the morphology of the invader is fractal, the saturation–pressure relation is system size dependent. Therefore, in a sense there is no such thing as a hydrodynamic ‘continuum scale’ in fractal systems. Our approach is thus rather a way to understand the problem at the relevant scales than a model for large scale continuum modelling. In real reservoir modelling, one also has to consider effects and problems not included in our theory. At larger length scales, inhomogeneities in the porous media are expected and will play an important role. This implies that the relevant length scales will be different in the different parts of the system. The invasion speed and thus the capillary number can vary in space and time. In addition, in three dimensional systems, gravity and fluid density differences can be very important. When dealing with systems where gravity is important, viscous effects will still be important (Hill 1952; Saffman and Taylor 1958; Méheust et al. 2002) and in this class of problems also the ratio of the relevant forces can be used to predict the relevant length scales of the displacement process (Wilkinson 1984; Chaouche et al. 1994a,b; Birov|jev et al. 1991; Méheust et al. 2002). Another limitation in our study is the high viscous contrast between the phases. In this respect, we would like to point out that there will generally be a high viscous contrast in systems where one of the phases is a gas, and that similar arguments have been successfully applied to systems where the viscous contrast were smaller (Frette et al. 1997; Aker et al. 2000).

In contrast to models used to describe standard water retention tests in soil samples, there are no semipermeable membranes at the inlet- and outlet-channel in the models used in this study. This makes it impossible to statically increase the pressure over the sample in order to reach the low water saturations commonly seen in published retention curves (Leverett 1941; Brooks and Corey 1964; Van Genuchten 1980; Lenhard et al. 1993; Hassanizadeh et al. 2002). This choice for our models was motivated by the idea that the lack of semi permeable

membranes has the advantage of being more ‘realistic’, in the sense that in real reservoir systems small volumes are *not* restricted by semi permeable membranes. On the contrary, when using semi permeable membranes the system can be forced into a state which is ‘out of reach’ in real systems where the application of a large pressure somewhere near a given sample volume would lead to the non-wetting liquid being forced into the surrounding porous medium, without further decrease of the water saturation in the sample volume in question.

6 Concluding Remarks

Results from drainage experiments on transparent quasi-two-dimensional porous models have been reported. The reduced data were used to obtain standard pressure–saturation curves.

By using different ways of driving the invasion process, we can control the dynamic component of the pressure head and explain the experimentally observed dynamic effects by relating them to theoretical arguments. Indeed, by combining detailed information on the displacement structure with global measurements of pressure and saturation, we have derived a scaling relation relating pressure, saturation, system size and the capillary number Ca . By applying this pressure–saturation scaling relation, curves for a range of capillary numbers have been collapsed onto a system size- and Ca -independent master capillary curve. We believe that this study can have a significant impact on the understanding of the impact of dynamic effects on retention curves, and it is our hope that that the size dependence could be applied in reservoir scale modelling.

Acknowledgments We would like to thank Henning A. Knudsen and Eirik G. Flekkøy for useful discussions and suggestions. We would also like to thank the Norwegian Research council for financial support of the project. Financial support for this research from the program REseau Alsace de Laboratoires en Ingénierie et Sciences pour l’Environnement (REALISE) is also gratefully acknowledged. R. T. and Y. M. acknowledge support from CNRS for traveling between France and Norway, under a french–norwegian PICS program.

Open Access This article is distributed under the terms of the Creative Commons Attribution Noncommercial License which permits any noncommercial use, distribution, and reproduction in any medium, provided the original author(s) and source are credited.

Appendix

A Pressure Adjustments

The ‘gravity pump’ used in the experiments consists of an open reservoir connected to the model and located a height H below the model (Méheust et al. 2002). The equation of motion for the liquid is:

$$\rho LA\phi \frac{dv}{dt} = \rho gHA - vR \quad (16)$$

where R is the total hydraulic resistance to flow. The total resistance is dominated by the resistance of the tube and valve connecting the model and the reservoir. We will therefore neglect the resistance of the porous medium. Solving the velocity $v(t)$ with the boundary conditions $v(t = 0) = 0$ and $v(t \gg T) = v_f$, one gets:

$$v(t) = \frac{gH\rho A}{R} (1 - e^{-\frac{tR}{\rho LA\phi}}) = v_f(1 - e^{-\frac{t}{T}}) \quad (17)$$

where $T = LA\phi\rho/R$ is a system specific relaxation time. By using Darcy's law and an effective pressure gradient set by the pressure drop exerted over the distance between the most advanced finger tip position $x = x_{\text{tip}}$ and the outlet at $x = L$ we get:

$$v = -\frac{\kappa}{\mu_w} \nabla P \simeq \frac{\kappa}{\mu_w} \frac{P}{L - x_{\text{tip}}} \quad (18)$$

Combining Eqs. 17 and 18, and the definition of the capillary number (1) yields:

$$P(t) = \frac{\mu_w}{\kappa} v_f(1 - e^{-\frac{t}{T}})(L - x_{\text{tip}}) \approx \frac{\text{Ca}\gamma}{a^2} (1 - e^{-\frac{t}{T}})(L - v_{\text{tip}}t) \quad (19)$$

where the speed of the advancing finger tip v_{tip} is assumed constant. The latter Eq. 19 can be used to correct for the initial pressure buildup. This is done by fitting Eq. 19 to the measured $P(t)$ with T and v_{tip} as fitting parameters. We estimate a single characteristic T by averaging the calculated T -values. This value is then used to correct for the initial pressure buildup, see Figs. 7 and 8.

References

- Aker, E., Måløy, K.J., Hansen, A.: Viscous stabilization of 2D drainage displacements with trapping. *Phys. Rev. Lett.* **84**(20), 4589–4592 (2000)
- Auradou, H., Måløy, K.J., Schmittbuhl, J., Hansen, A.: Drainage in a rough gouge-filled fracture. *Transp. Porous Media* **50**, 267–305 (2003)
- Auradou, H., Måløy, K.J., Schmittbuhl, J., Hansen, A., Bideau, D.: Competition between correlated buoyancy and uncorrelated capillary effects during drainage. *Phys. Rev. E* **60**(6), 7224–7234 (1999)
- Bear, J.: *Dynamics of Fluids in Porous Media*. American Elsevier Publishing Company, New York (1972)
- Birovljev, A., Furuberg, L., Feder, J., Jøssang, T., Måløy, K.J., Aharony, A.: Gravity invasion percolation in 2 dimensions—experiment and simulation. *Phys. Rev. Lett.* **67**(5), 584–587 (1991)
- Bohy, M., Dridi, L., Schäfer, G., Razakarisoa, O.: Transport of a mixture of chlorinated solvent vapors in the vadose zone of a sandy aquifer. *Vadose Zone J.* **5**, 539–553 (2006)
- Bourgeat, A., Panfilov, M.: Effective two-phase flow through highly heterogeneous porous media: capillary nonequilibrium effects. *Computat. Geosci.* **2**(3), 191–215 (1998)
- Brooks, R.H., Corey, A.T.: *Hydraulic Properties of Porous Media Hydrology Paper 3*. Colorado State University, Fort Collins, Colorado (1964)
- Chandler, R., Koplik, J., Lerman, K., Willemsen, J.F.: Capillary displacement and percolation in porous media. *J. Fluid Mech.* **119**, 249–267 (1982)
- Chaouche, M., Rakotomalala, N., Salin, D., Xu, B., Yortsos, Y.C.: Invasion percolation in a hydrostatic or permeability gradient: experiments and simulations. *J. Fluid Mech.* **119**, 249–267 (1994a)
- Chaouche, M., Rakotomalala, N., Salin, D., Xu, B., Yortsos, Y.C.: Invasion percolation in a hydrostatic or permeability gradient: experiments and simulations. *Phys. Rev. E* **49**(5), 4133–4139 (1994b)
- Dahle, H.K., Celia, M.A., Hassanizadeh, S.M.: Bundle-of-tubes model for calculating dynamic effects in the capillary-pressure-saturation relationship. *Transp. Porous Media* **58**(1–2), 5–22 (2005)
- Dullien, F.A.L.: *Porous Media Fluid Transport and Pore Structure*, 2nd edn. Academic Press Inc, San Diego (1992)
- Feder, J.: *Fractals*. Plenum Press, New York (1988)
- Frette, O.I., Måløy, K.J., Schmittbuhl, J., Hansen, A.: Immiscible displacement of viscosity-matched fluids in two-dimensional porous media. *Phys. Rev. E* **55**(3), 2969–2975 (1997)
- Furuberg, L., Måløy, K.J., Feder, J.: Intermittent behavior in slow drainage. *Phys. Rev. E* **53**(1), 966–977 (1996)
- Hassanizadeh, S.M., Gray, W.: High-velocity flow in porous-media by Hassanizadeh and Gray—Reply. *Transp. Porous Media* **3**(3), 319–321 (1988)
- Hassanizadeh, S.M., Celia, M.A., Dahle, H.K.: Dynamic effect in the capillary pressure—saturation relationship and its impacts on unsaturated flow. *Vadose Zone J.* **1**, 38–57 (2002)
- Helmig, R.: *Multiphase Flow and Transport Processes in the Subsurface, A Contribution to the Modeling of Hydrosystems*. Springer (Environmental Engineering), Berlin (1997)

- Hill, S.: Channelling in packed columns. *Chem. Eng. Sci.* **1**, 247–253 (1952)
- Homsy, G.M.: Viscous fingering in porous media. *Annu. Rev. Fluid Mech.* **19**, 271–311 (1987)
- Hulin, J.P., Clément, E., Baudet, C., Gouyet, J.F., Rosso, M.: Quantitative analysis of an invading-fluid front under gravity. *Phys. Rev. Lett.* **61**(3), 333–336 (1987)
- Kool, J.B., Parker, J.C.: Development and evaluation of closed form expressions for hysteretic soil hydraulic properties. *Water Resour. Res.* **23**, 105–114 (1987)
- Lenhard, R.J., Johnson, T.G., Parker, J.C.: Experimental observations of nonaqueous-phase liquid subsurface movement. *J. Contam. Hydrol.* **24**, 79–101 (1993)
- Lenormand, R.: Flow through porous media: limits of fractal patterns. *Proc. R. Soc. Lond. A* **423**, 159–168 (1989)
- Lenormand, R., Zarcone, C.: Invasion percolation in an etched network: measurement of a fractal dimension. *Phys. Rev. Lett.* **54**(20), 2226–2229 (1985)
- Lenormand, R., Zarcone, C.: Capillary fingering: percolation and fractal dimension. *Transp. Porous Media* **4**, 599–612 (1989)
- Lenormand, R., Zarcone, C., Sarr, A.: Mechanisms of the displacement of one fluid by another in a network of capillary ducts. *J. Fluid Mech.* **135**, 337–353 (1983)
- Lenormand, R., Touboul, E., Zarcone, C.: Numerical models and experiments on immiscible displacement in porous media. *J. Fluid Mech.* **189**, 165–187 (1988)
- Leverett, M.C.: Capillary behaviour in porous solids. *Trans. AIME* **142**, 152–169 (1941)
- Løvøll, G., Méheust, Y., Toussaint, R., Schmittbuhl, J., Måløy, K.J.: Growth activity during fingering in a porous Hele-Shaw cell. *Phys. Rev. E* **70**(2), 026301 (2004)
- Luckner, L., Van Genuchten, M.T.H.: A consistent set of parametric models for the two-phase flow of immiscible fluids in the subsurface. *Water Resour. Res.* **25**, 2187–2193 (1989)
- Måløy, K.J., Feder, J., Jøssang, T.: Viscous fingering fractals in porous media. *Phys. Rev. Lett.* **55**, 2688–2691 (1985)
- Måløy, K.J., Furuberg, L., Feder, J., Jøssang, T.: Dynamics of slow drainage in porous-media. *Phys. Rev. Lett.* **68**(14), 2161–2164 (1992)
- Mandelbrot, B.B.: *The Fractal Geometry of Nature*. W.H. Freeman, New York (1982)
- Méheust, Y., Løvøll, G., Måløy, K.J., Schmittbuhl, J.: Interface scaling in a 2D porous medium under combined viscous, gravity and capillary effects. *Phys. Rev. E* **66**, 51603–51615 (2002)
- Mualem, Y.: A new model for predicting the hydraulic conductivity of unsaturated porous media. *Water Resour. Res.* **12**, 512–513 (1976)
- Mualem, Y.: A modified depend-domain theory of hysteresis. *Soil Sci.* **137**, 283–291 (1984)
- Niessner, J., Hassanizadeh, S.M.: A model for two-phase flow in porous media including fluid-fluid interfacial area. *Water Resour. Res.* **44**(8), w08439 (2008). doi:[10.1029/2007WR006721](https://doi.org/10.1029/2007WR006721)
- Parker, J.C., Lenhard, R.J.: Model for hysteretic constitutive relations governing multiphase flow 1 Saturation-pressure relations. *Water Resour. Res.* **23**, 2187–2196 (1987a)
- Parker, J.C., Lenhard, R.J., Kuppusami, T.: A parametric model for constitutive properties governing multiphase flow in porous media. *Water Resour. Res.* **23**, 618–624 (1987b)
- Poulaivissilis, A.: Hysteresis of pore water, an application of concept of independent domains. *Soil Sci.* **93**, 405–412 (1962)
- Saffman, P.G., Taylor, G.: The penetration of a fluid into a porous medium or Hele-Shaw cell containing a more viscous liquid. *Proc. Soc. Lond. Ser. A* **245**, 312–329 (1958)
- Sahimi, M.: *Flow and Transport in Porous Media and Fractured Rock*. VCH Verlagsgesellschaft mbH, Weinheim, Germany (1995)
- Schmittbuhl, J., Hansen, A., Auradou, H., Måløy, K.J.: Geometry and dynamics of invasion percolation with correlated buoyancy. *Phys. Rev. E* **61**(4), 3985–3995 (2000)
- Smiles, D., Vachaud, G., Vaucelin, M.: A test of the uniqueness of the soil moisture characteristics during transient non-hysteretic flow of water in a rigid soil. *Soil Sci. Soc. Am. J.* **35**, 534–539 (1971)
- Stauffer, F.: Einfluss der kapillaren Zone auf instationäre Drainagevorgänge, Bericht R 13–77 (Diss ETH Nr. 5931). IHW ETH Zürich (1977)
- Stauffer, F., Kinzelbach, W.: Cyclic hysteretic flow in porous medium column: model, experiment, and simulations. *J. Hydrol.* **240**, 264–275 (2001)
- Toussaint, R., Løvøll, G., Meheust, Y., Måløy, K.J., Schmittbuhl, J.: Influence of pore-scale disorder on viscous fingering during drainage. *Europhys. Lett.* **71**(4), 583–589 (2005)
- Van Genuchten, M.T.: A closed-form equation for predicting the hydraulic conductivity of unsaturated soils. *Soil Sci. Soc. Am. J.* **44**, 892–898 (1980)
- Vedvik, A., Wagner, G., Oxaal, U., Feder, J., Meakin, P., Jøssang, T.: Fragmentation Transition for Invasion Percolation in Hydraulic Gradients. *Phys. Rev. Lett.* **80**(14), 3065–3068 (1998)
- Washburn, E.W.: The dynamics of capillary flow. *Phys. Rev.* **17**, 273–283 (1921)

-
- Weitz, D.A., Stokes, J.P., Ball, R.C., Kushnick, A.P.: Dynamic capillary-pressure in porous media—origin of the viscous fingering length scale. *Phys. Rev. Lett.* **59**(26), 2967–2970 (1987)
- Wilkinson, D.: Percolation model of immiscible displacement in the presence of buoyancy forces. *Phys. Rev. A* **34**(1), 520–531 (1984)
- Wilkinson, D., Willemsen, J.F.: Invasion percolation: a new form of percolation theory. *J. Phys. A* **16**, 3365–3376 (1983)
- Xu, B., Yortsos, Y.C., Salin, D.: Invasion percolation with viscous forces. *Phys. Rev. E* **57**(1), 739–751 (1998)
- Yortsos, Y.C., Xu, B., Salin, D.: Phase diagram of fully developed drainage in porous media. *Phys. Rev. Lett.* **79**(23), 4581–4584 (1997)